Advances in Concrete Construction, *Vol. 9, No. 3 (2020) 327-335*
DOI: https://doi.org/10.12989/acc.2020.9.3.327

Dynamic stress response in the nanocomposite concrete pipes with internal fluid under the ground motion load

Behrooz Keshtegar[1,2a], Javad Tabatabaei[3], Reza Kolahchi*[4] and Nguyen-Thoi Trung[1,2]

[1]*Division of Computational Mathematics and Engineering, Institute for Computational Science, Ton Duc Thang University, Ho Chi Minh City, Viet Nam*
[2]*Faculty of Civil Engineering, Ton Duc Thang University, Ho Chi Minh City, Viet Nam*
[3]*Department of petroleum engineering and geology, Meymeh branch, Islamic Azad University, Meymeh, Iran*
[4]*Institute of Research and Development, Duy Tan University, Da Nang 550000, Viet Nam*

(*Received December 8, 2019, Revised February 14, 2020, Accepted February 17, 2020*)

Abstract. Concrete pipes are considered important structures playing integral role in spread of cities besides transportation of gas as well as oil for far distances. Further, concrete structures under seismic load, show behaviors which require to be investigated and improved. Therefore, present research concerns dynamic stress and strain alongside deflection assessment of a concrete pipe carrying water-based nanofluid subjected to seismic loads. This pipe placed in soil is modeled through spring as well as damper. Navier-Stokes equation is utilized in order to gain force created via fluid and, moreover, mixture rule is applied to regard the influences related to nanoparticles. So as to model the structure mathematically, higher order refined shear deformation theory is exercised and with respect to energy method, the motion equations are obtained eventually. The obtained motion equations will be solved with Galerkin and Newmark procedures and consequently, the concrete pipe's dynamic stress, strain as well as deflection can be evaluated. Further, various parameters containing volume percent of nanoparticles, internal fluid, soil foundation, damping and length to diameter proportion of the pipe and their influences upon dynamic stress and strain besides displacement will be analyzed. According to conclusions, increase in volume percent of nanoparticles leads to decrease in dynamic stress, strain as well as displacement of structure.

Keywords: dynamic response; soil medium; fluid; damping; nanoparticles

1. Introduction

Without doubt, improvement and spread of cities require infrastructures which can fulfil humankind's needs and therefore, specifically, concrete pipes are considered one of these infrastructures which play important role in satisfying the requirements of metropolises. These structures are useful for irrigation, water supply lines, storm drains and so on. In fact, their striking traits include corrosion resistance, smooth face and high pressure durability. As a result, engineers and researchers are encouraged to investigate mechanical behavior of such structure. Al Rikabi *et al*. (2019) reported a pipe reinforced by synthetic fibers utilizing three-edge bearing test. It is clarified that reinforcement can rise stiffness, flexibility and cracking load and decline the manufacturing cost. (Goldaran *et al*. 2020) conducted a research regarding a technique by which the corrosion of prestressed concrete pipe can be detected. Hence, they introduced acoustic emission method and water pressure was considered variably and both dry and wet conditions were regarded. They ascertained that the presented technique is dependable and efficient procedure to identify created corrosion. (Rose *et al*. 2018) analyzed healing of concrete pipe leaks. In this paper, they declared that favorable water would be efficient for concrete pipes to be healed autogenously while unfavorable water can worsen this process. They expressed that healing method integrally needs solution having supersaturated quantities of calcium carbonate. In another paper, Feng *et al*. (2015) reported a novel way in order to identify cracks and leakages in concrete pipes and monitor them. In fact, they embed a piezoceramic in the concrete pipe and they can act as sensor and actuator by which the cracks can be detected. Further, circumferential and axial cracks have been analyzed. Nouri (2017) analyzed vibration as well as stability of a concrete pipe carrying fluid and considered carbon nanotubes (CNTs) as reinforcement. This structure is under magnetic field and various parameters such as velocity of fluid, CNT volume fraction and their geometry have been discussed. In another paper, Peyvandi *et al*. (2013) carried out a research regarding diverse fiber reinforcements affecting positively performance and effectiveness of concrete pipes besides their experimental investigations. They declared that various synthetic fibers including aramid, carbon and AR-glass have been analyzed and virtually these fibers could ameliorate properties of concrete pipes such as shear resistance and reduction of weights. Nonlinear natural frequency of FG-CNT sandwich plate in thermal environment is analyzed by Mehar *et al*. (2017). Influence of thermal loads upon vibration of structure is discussed accurately. Moreover, FEM is used for solution of motion

*Corresponding author, Ph.D.
E-mail: rezakolahchi@duytan.edu.vn
[a]Professor
E-mail: beh.keshtegar@tdtu.edu.vn

http://www.techno-press.org/?journal=acc&subpage=7
ISSN: 2287-5301 (Print), 2287-531X (Online)

equations. Panda and Singh (2009) investigated post-buckling analysis of laminated shallow panel. So as to utilize them expeditiously, science of their either static or dynamic behaviors used in process of manufacturing would be essential. Panda and Singh (2013) reported free vibration of a post-buckled laminated composite shell. The governing equations are derived using Hamilton's principle and solved by FEM. Katariya *et al*. (2017) carried out a research about thermal buckling load of sandwich panel. In addition to obtaining and solving the governing equations using higher order theory and FEM respectively, influences of structural variables upon critical buckling load are discovered. In agreement with this subject, in another paper, buckling of a FG-CNTRC sandwich shell in thermal environment is investigated by Mehar *et al*. (2019). The outcomes have been indicating that negative Poisson's proportion core leads to lower bending moment compared with the positive Poisson's proportion core. Vibration analysis of FG-CNT sandwich panel in thermal environment is conducted by Mehar and Panda (2017).

Nowadays, the earthquake phenomenon has received attentions due to the dangers threatening huge areas in the world. In spite of numerous researches regarding protection against earthquakes alongside tremors, the governments give importance to this phenomenon for saving people and reinforcing infrastructures. Therefore, analyzing and consequently, strengthening various structures used in cities, in particular in the soil, is pivotal. Kormanikova and Kotrasova (2018) discussed a laminated composite cylindrical reservoir subjected to seismic load. They accentuated this research because of considering impulsive and hydrodynamic besides hydrostatic pressures upon tanks. Further, first order shear deformation theory is applied. Hajmohammad *et al*. (2018) investigated an underwater concrete structure subjected to seismic load carrying fluid. In order to improve the performance of this structure, it has been reinforced via polymer nanofibers. Utilizing Hamilton's principle and differential quadrature (DQ) method, governing equations are derived and solved. Further, nanofiber volume fraction and agglomeration have been discussed. Ma and Zhang (2016) analyzed a prestressed wind tower composed of concrete under seismic load. It was found that in comparison with the traditional steel towers, the seismic load with mode damping ration related to the supposed concrete structure would not be considerable. Montuori and Muscati (2016) discussed a notable and novel model for designing resistant concrete frames against seismic load. In fact, such structures show advanced behaviors against earthquake load. Taherifar *et al*. (2018) carried out a research as to concrete structure having smart layer subjected to seismic load. In this work, Navier-Stokes equation is utilized to evaluate the created force between pipe and fluid. In this work, SiO2 nanoparticles volume fraction and aspect ratio are discussed. It should be noted that DQ method is applied for solution of governing equations. Looi *et al*. (2017) analyzed seismic behavior of reinforced concrete walls. In addition, this research studies effect of axial load ratio with short shear span. Luo *et al*. (2020) presented depiction of concrete systems subjected to far fault earthquakes.

Numerical methods play prominent role in solving

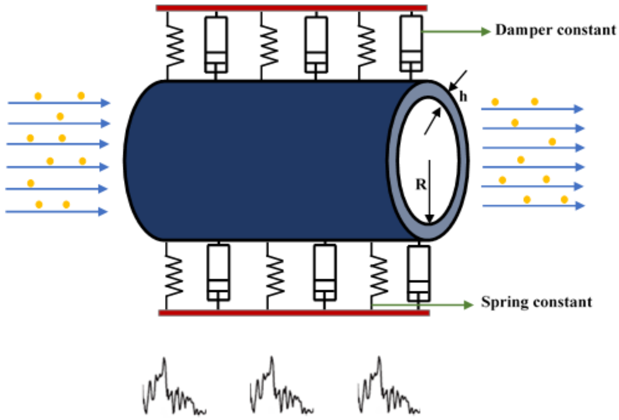

Fig. 1 Configuration of concrete pipe carrying water-based nanofluid buried in soil foundation subjected to seismic load

governing equations and the trait that can attach importance to them, is accuracy. In this paper, Galerkin method has been utilized and there are numerous articles published using this method. Heydari Nosrat Abadi and Zamani Nouri (2019) analyzed pipes conveying fluid in thermal environment using Galerkin method. They indicated that this numerical method has accurate results. Hua *et al*. (2018) investigated natural frequency of cantilever beam utilizing Galerkin procedure. In this research, the results are compared with other papers and show perfect accuracy of obtained results as well. Karimi and Shahidi (2018) carried out a research regarding buckling of skew nanoplate employing Galerkin procedure. They have tested the results using this procedure with Navier's solution for showing the precision. Belardi *et al*. (2018) discussed bending of composite circular plate using Galerkin method. Azmi *et al*. (2019) applied differential quadrature solution for dynamic analysis of concrete beam containg nanoparticles.

Hitherto, there is no paper investigating dynamic stress, strain and displacement evaluation of a concrete pipe carrying water-based nanofluid subjected to seismic load. This structure is located in soil and it is simulated via spring and damper. In order to achieve the force between fluid and pipe, Navier-Stokes equation is utilized. For modeling this structure mathematically, higher order refined shear deformation theory is applied and using Hamilton's principle, governing equations are obtained and solved utilizing Galerkin as well as Newmark procedures. The influence of various parameters such as nanoparticle volume fraction, soil medium and internal fluid upon dynamic stress, strain and deflection are discussed.

2. Problem definition

Fig. 1 illustrates a concrete pipe carrying water-based nanofluid buried in the soil regarding damping of the soil. As observed, this concrete structure is subjected to axial earthquake loads.

With respect to higher order refined shear deformation theory for shell, displacement vectors are given by Thai and Choi (2011)

$$U(x,\theta,z,t)=u\ (x,\theta,t)-z\ \frac{\partial}{\partial x}w_b(x,\theta,t)+z\left[\frac{1}{4}-\frac{5}{3}\left(\frac{z}{h}\right)^2\right]\frac{\partial}{\partial x}w_s(x,\theta,t),\tag{1}$$

$$V(x,\theta,z,t)=v\ (x,\theta,t)-z\ \frac{\partial}{R\partial\theta}w_b(x,\theta,t)+z\left[\frac{1}{4}-\frac{5}{3}\left(\frac{z}{h}\right)^2\right]\frac{\partial}{R\partial\theta}w_s(x,\theta,t),\tag{2}$$

$$W(x,\theta,z,t)=w_b(x,\theta,t)+w_s(x,\theta,t),\tag{3}$$

in which u and v respectively describe the mid-plane displacements in the x and θ directions; w_s and w_b respectively express shear as well as bending transverse deflections. Furthermore, the strain components of this concrete structure are described as

$$\varepsilon_{xx}=\frac{\partial u}{\partial x}-z\ \frac{\partial^2 w_b}{\partial x^2}-f\ \frac{\partial^2 w_s}{\partial x^2},\tag{4}$$

$$\varepsilon_{\theta\theta}=\frac{\partial v}{\partial x}+\frac{w_b}{R}+\frac{w_s}{R}-z\ \frac{\partial^2 w_b}{R^2\partial\theta^2}-f\ \frac{\partial^2 w_s}{R^2\partial\theta^2},\tag{5}$$

$$\gamma_{x\theta}=\frac{\partial v}{\partial x}+\frac{\partial u}{R\partial\theta}-2z\ \frac{\partial^2 w_b}{R\partial x\,\partial\theta}-2f\ \frac{\partial^2 w_s}{R\partial x\,\partial\theta},\tag{6}$$

$$\gamma_{xz}=g\ \frac{\partial w_s}{\partial x},\tag{7}$$

$$\gamma_{\theta z}=g\ \frac{\partial w_s}{R\partial\theta},\tag{8}$$

in which $f=-\frac{z}{4}+\frac{5}{3}z\left(\frac{z}{h}\right)^2$ and $g=\frac{5}{4}-5\left(\frac{z}{h}\right)^2$.

The constitutive relation for the stress can be written as below

$$\begin{Bmatrix}\sigma_{xx}\\ \sigma_{\theta\theta}\\ \sigma_{\theta z}\\ \sigma_{zx}\\ \sigma_{x\theta}\end{Bmatrix}=\begin{bmatrix}C_{11}&C_{12}&0&0&0\\ C_{21}&C_{22}&0&0&0\\ 0&0&C_{44}&0&0\\ 0&0&0&C_{55}&0\\ 0&0&0&0&C_{66}\end{bmatrix}\begin{Bmatrix}\varepsilon_{xx}\\ \varepsilon_{\theta\theta}\\ \gamma_{\theta z}\\ \gamma_{xz}\\ \gamma_{x\theta}\end{Bmatrix},\tag{9}$$

in which C_{ij} (i,j=1,2,…,6) defines stiffness constants.

2.1 Kinetic energy

The kinetic energy related to this concrete pipe can be given by

$$K=\frac{\rho}{2}\int_{\Omega_0}\int_{-h/2}^{h/2}\left(\left(\frac{\partial u}{\partial t}-z\ \frac{\partial^2 w_b}{\partial t\,\partial x}-f\ \frac{\partial^2 w_s}{\partial t\,\partial x}\right)^2+\left(\frac{\partial v}{\partial t}-z\ \frac{\partial^2 w_s}{R\partial t\,\partial\theta}-f\ \frac{\partial^2 w_s}{R\partial t\,\partial\theta}\right)^2+\left(\frac{\partial w_b}{\partial t}+\frac{\partial w_s}{\partial t}\right)^2\right)dV,\tag{10}$$

in which ρ hints at density of pipe.

2.2 Potential energy

Likewise, the potential energy for assumed concrete structure is written as below

$$\begin{aligned}U=\frac{1}{2}\int_{\Omega_0}\Bigg(&N_{xx}\frac{\partial u}{\partial x}+N_{\theta\theta}\left(\frac{\partial v}{\partial\theta}+\frac{w}{R}\right)+Q_\theta\frac{\partial w_s}{R\partial\theta}+Q_x\frac{\partial w_s}{\partial x}+N_{x\theta}\left(\frac{\partial v}{\partial x}+\frac{\partial u}{R\partial\theta}\right)\\&+M_{xx}^b\frac{\partial^2 w_b}{\partial x^2}+M_{\theta\theta}^b\frac{\partial^2 w_b}{R^2\partial\theta^2}+M_{x\theta}^b\frac{\partial^2 w_b}{R\partial x\,\partial\theta}+M_{xx}^s\frac{\partial^2 w_s}{\partial x^2}\\&+M_{\theta\theta}^s\frac{\partial^2 w_s}{R^2\partial\theta^2}+M_{x\theta}^s\frac{\partial^2 w_s}{R\partial x\,\partial\theta}\Bigg)dxRd\theta,\end{aligned}\tag{11}$$

in which stress resultants can be expressed as

$$\begin{Bmatrix}N_i\\ M_i^b\\ M_i^s\end{Bmatrix}=\int_{-h/2}^{h/2}\begin{bmatrix}1\\ z\\ f\end{bmatrix}\sigma_i dz,\quad (\mathrm{i}=\mathrm{xx},\theta\theta,\mathrm{x}\theta)\tag{12}$$

$$Q_i=\int_{-h/2}^{h/2}g\sigma_i dz,\quad (\mathrm{i}=\mathrm{x}z,\theta z)\tag{13}$$

2.3 External work

It should be noted that the work done contains soil foundation, internal fluid as well as earthquake load.

2.3.1 Soil foundation

The work done by means of soil foundation is given by

$$W_s=\int_A\left(-k_sW-c_d\dot{W}\right)WdA,\tag{14}$$

in which k_s and c_d respectively represent coefficient of soil spring and damping of soil foundation.

2.3.2 Earthquake load

The external work related to the seismic force is given by

$$W_e=\int_A\left(ma(\mathrm{t})\mathrm{u}\right)dA,\tag{15}$$

in which $a(t)$ and m respectively define acceleration as well as mass.

2.3.3 Internal fluid

In this part, the widely known Navier-Stokes equation is expressed as below

$$\rho_f\frac{d\mathbf{V}}{dt}=-\nabla\mathbf{P}+\mu\nabla^2\mathbf{V}+\mathbf{F}_{body},\tag{16}$$

in which $V\equiv(v_z,v_\theta,v_x)$ describes flow velocity vector assumed in cylindrical coordinate system among x, θ and z directions. Moreover, P, μ and ρ_f respectively represent the fluid's pressure, the fluid's viscosity and the fluid's density and F_{body} expresses the body forces. Likewise, based on Navier-Stokes equation, total derivative operator according to t is

$$\frac{d}{dt}=\frac{\partial}{\partial t}+v_x\frac{\partial}{\partial x}+v_\theta\frac{\partial}{R\partial\theta}+v_z\frac{\partial}{\partial z}, \quad (17)$$

It is worth declaring that the contact point amid fluid and core, the relative velocity as well as acceleration in radial direction are considered equal. Therefore

$$v_z=\frac{dw}{dt}, \quad (18)$$

By utilizing Eqs. (17) and (18) and introducing into Eq. (16), the pressure created inside pipe is calculated as

$$\begin{aligned}\frac{\partial p_z}{\partial z}&=-\rho_f\left(\frac{\partial^2 w}{\partial t^2}+2v_x\frac{\partial^2 w}{\partial x\partial t}+v_x{}^2\frac{\partial^2 w}{\partial x^2}\right)\\&+\mu\left(\frac{\partial^3 w}{\partial x^2\partial t}+\frac{\partial^3 w}{R^2\partial\theta^2\partial t}+v_x\left(\frac{\partial^3 w}{\partial x^3}+\frac{\partial^3 w}{R^2\partial\theta^2\partial x}\right)\right),\end{aligned} \quad (19)$$

In this section, multiplying the whole Eq. (19) in the inside pipe's area, A, the radial force in the pipe is counted as below

$$\begin{aligned}F_{fluid}=A\frac{\partial p_z}{\partial z}&=-\rho_f\left(\frac{\partial^2 w}{\partial t^2}+2v_x\frac{\partial^2 w}{\partial x\partial t}+v_x{}^2\frac{\partial^2 w}{\partial x^2}\right)\\&+\mu\left(\frac{\partial^3 w}{\partial x^2\partial t}+\frac{\partial^3 w}{R^2\partial\theta^2\partial t}+v_x\left(\frac{\partial^3 w}{\partial x^3}+\frac{\partial^3 w}{R^2\partial\theta^2\partial x}\right)\right),\end{aligned} \quad (20)$$

Eventually, the external work relative to fluid pressure is written as below

$$\begin{aligned}W_f&=\int(F_{fluid})wdA=\int\left(-\rho_{eff}\left(\frac{\partial^2 w}{\partial t^2}+2v_x\frac{\partial^2 w}{\partial x\,\partial t}+v_x{}^2\frac{\partial^2 w}{\partial x^2}\right)\right.\\&\left.+\mu_{eff}\left(\frac{\partial^3 w}{\partial x^2\partial t}+\frac{\partial^3 w}{R^2\partial\theta^2\partial t}+v_x\left(\frac{\partial^3 w}{\partial x^3}+\frac{\partial^3 w}{R^2\partial\theta^2\partial x}\right)\right)\right)wdA,\end{aligned} \quad (21)$$

in which water-nanoparticle flow's effective viscosity, $\mu_{\mu_{eff}}$, as well as density, $\rho_{\mu_{eff}}$, may be achieved through mixture law for Al_2O_3 nanoparticles considering diameter of 13 (nm) as follows

$$\rho_{eff}=\phi\rho_n+(1-\phi)\rho_f, \quad (22)$$

$$\mu_{eff}=(1+39.11\varphi+533.9\varphi^2)\mu_f, \quad (23)$$

in which ρ_n, ρ_f, μ_n, μ_f and ϕ respectively define nanoparticle's density, fluid's density, nanoparticle's viscosity, fluid's viscosity and volume percent of nanoparticle.

2.4 Governing equations

With respect to the Hamilton's principle and the relations obtained in above sections, the governing equations are derived as below

$$\int_0^t(\delta U-\delta W_f-\delta W-\delta W_e-\delta K)dt=0. \quad (24)$$

By introducing Eqs. (10), (11), (14), (15) and (21) into Eq. (24), governing equations can be extended as below

$$\delta u:\frac{\partial N_{xx}}{\partial x}+\frac{\partial N_{x\theta}}{R\partial\theta}=I_0\frac{\partial^2 u}{\partial t^2}-I_1\frac{\partial^3 w_b}{\partial t^2\partial x}-J_1\frac{\partial^3 w_s}{\partial t^2\partial x}+ma_x(\mathrm{t}), \quad (25)$$

$$\delta v:\frac{\partial N_{x\theta}}{\partial x}+\frac{\partial N_{\theta\theta}}{R\partial\theta}=I_0\frac{\partial^2 v}{\partial t^2}-I_1\frac{\partial^3 w_b}{R\partial t^2\partial\theta}-J_1\frac{\partial^3 w_s}{R\partial t^2\partial\theta}, \quad (26)$$

$$\begin{aligned}&\delta w_b:\frac{\partial^2 M_{xx}^b}{\partial x^2}+2\frac{\partial^2 M_{x\theta}^b}{R\partial x\partial\theta}+\frac{\partial^2 M_{\theta\theta}^b}{R^2\partial\theta^2}-\frac{N_{\theta\theta}}{R}\\&+P_{Fluid}-k_s(w_b+w_s)-c_d(\dot w_b+\dot w_s)=\\&I_0\left(\frac{\partial^2 w_b}{\partial t^2}+\frac{\partial^2 w_s}{\partial t^2}\right)+I_1\left(\frac{\partial^3 u}{\partial t^2\partial x}+\frac{\partial^3 v}{R\partial t^2\partial\theta}\right)\\&-I_2\nabla^2\left(\frac{\partial^2 w_b}{\partial t^2}\right)-J_2\nabla^2\left(\frac{\partial^2 w_s}{\partial t^2}\right),\end{aligned} \quad (27)$$

$$\begin{aligned}&\delta w_s:\frac{\partial^2 M_{xx}^s}{\partial x^2}+2\frac{\partial^2 M_{x\theta}^s}{R\partial x\partial\theta}+\frac{\partial^2 M_{\theta\theta}^s}{R^2\partial\theta^2}-\frac{N_{\theta\theta}}{R}\\&+\frac{\partial Q_{xz}}{\partial x}+\frac{\partial Q_{x\theta}}{R\partial\theta}+P_{Fluid}-c_d(\dot w_b+\dot w_s)=\\&I_0\left(\frac{\partial^2 w_b}{\partial t^2}+\frac{\partial^2 w_s}{\partial t^2}\right)+I_1\left(\frac{\partial^3 u}{\partial t^2\partial x}+\frac{\partial^3 v}{R\partial t^2\partial\theta}\right)\\&-J_2\nabla^2\left(\frac{\partial^2 w_b}{\partial t^2}\right)-K_2\nabla^2\left(\frac{\partial^2 w_s}{\partial t^2}\right),\end{aligned} \quad (28)$$

in which

$$I_i=\int_{-h/2}^{h/2}\rho z^i dz \qquad (i=0,1,2), \quad (29)$$

$$J_i=-\frac{1}{4}I_i+\frac{5}{3h^2}I_{i+2} \qquad (i=1,2), \quad (30)$$

$$K_2=\frac{1}{16}I_2-\frac{5}{6h^2}I_4+\frac{25}{9h^4}I_6. \quad (31)$$

Furthermore, the extended stress resultants are presented in Appendix A.

3. Solving method

According to the procedure recommended by Galerkin (Zamani Nouri 2018), yields

$$\mathbf{d}=\begin{Bmatrix}u\\v\\w_b\\w_s\end{Bmatrix}=\sum_{m=0}^{\infty}\sum_{n=0}^{\infty}\begin{Bmatrix}A_1\cos(\frac{m\pi x}{a})\sin(n\theta)\cos(\omega t)\\A_2\sin(\frac{m\pi x}{a})\cos(n\theta)\cos(\omega t)\\A_3\sin(\frac{m\pi x}{a})\sin(n\theta)\cos(\omega t)\\A_4\sin(\frac{m\pi x}{a})\sin(n\theta)\cos(\omega t)\end{Bmatrix}, \quad (32)$$

in which ω mentions frequency, n and m respectively describe circumferential as well as half axial wave numbers. Hence, the governing equations can be given by

$$\left([K]\{d\}+[C]\{\dot d\}+[M]\{\ddot d\}\right)=\{F\}, \quad (33)$$

in which [K], [C] and [M] respectively refer to the stiffness, damping and mass matrices. Further, $\{d\}=\{u,v,w_b,w_s\}$, defines the displacement vector. Based on the procrdure of Newmark (Simsek 2010), the Eq. (33) can be written as following form

$$\left[K_L+K_{NL}(d_{i+1})+\alpha_0 M+\alpha_1 C\right](d_{i+1})=$$

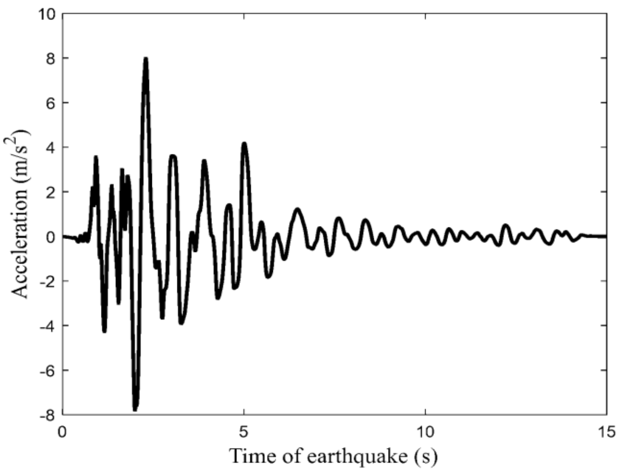

Fig. 2 Acceleration of Kobe earthquake

$$\left[Q_{i+1}+M\left(\alpha_0 d_i+\alpha_2\dot{d}_i+\alpha_3\ddot{d}_i\right)+C\left(\alpha_1 d_i+\alpha_4\dot{d}_i+\alpha_5\ddot{d}_i\right)\right], \tag{34}$$

in which subscript, i+1, demonstrates time $t=t_{i+1}$; $\dot{d}$ and $\ddot{d}$ respectively represent structure's velocity and acceleration and are expressed as

$$\ddot{d}_{i+1}=\alpha_0(d_{i+1}-d_i)-\alpha_2\dot{d}_i-\alpha_3\ddot{d}_i, \tag{35}$$

$$\dot{d}_{i+1}=\dot{d}_i+\alpha_6\ddot{d}_i+\alpha_7\ddot{d}_{i+1}, \tag{36}$$

in which

$$\begin{gathered}\alpha_0=\frac{1}{\chi\Delta t^2},\quad \alpha_1=\frac{\gamma}{\chi\Delta t},\quad \alpha_2=\frac{1}{\chi\Delta t},\\ \alpha_3=\frac{1}{2\chi}-1,\quad \alpha_4=\frac{\gamma}{\chi}-1,\ \alpha_5=\frac{\Delta t}{2}\left(\frac{\gamma}{\chi}-2\right),\\ \alpha_6=\Delta t(1-\gamma),\quad \alpha_7=\Delta t\gamma,\end{gathered} \tag{37}$$

where γ=0.5 and χ=0.25. Utilizing iteration method, Eq. (33) is solved.

4. Results and discussion

In present part, so as to evaluate obtained results of this research focusing upon particular parameters, a concrete pipe is chosen with Young's modulus of E=20 GPa. Further, the Poisson's ratio, length to diameter ratio and thickness to radius ratio of pipe respectively are considered v=0.3, L/D=1 and h/R=0.01. The internal fluid material is water with density, ρ_f=998.2 kg/m^3, and viscosity, μ_f=1.003×10^{-3} Ns/m^2, integrated with the nanoparticles, Al_2O_3, with density, ρ_f=3970 kg/m^3. Moreover, the supposed spring constant related to soil foundation is calculated using following formulation (Bowles 1988)

$$k_s=\frac{2E_s}{\left(1-v_s^2\right)+2H/B}. \tag{38}$$

In the above relation, E_S and v_S respectively express Young's modulus of soil and Poisson's ratio of soil; B and H respectively represent soil's width and height.

Likewise, the earthquake location is Kobe having the acceleration illustrated in Fig. 2.

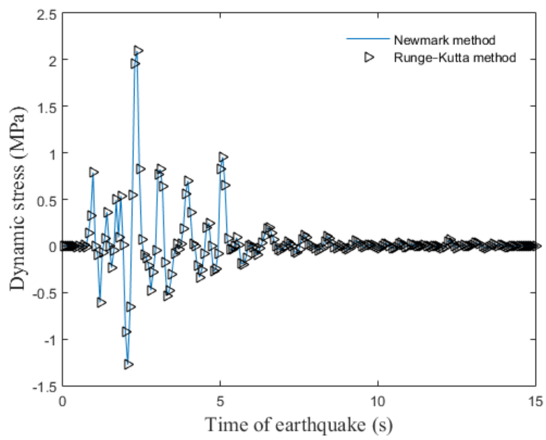

Fig. 3(a) Effect of nanoparticle volume fraction upon dynamic stress

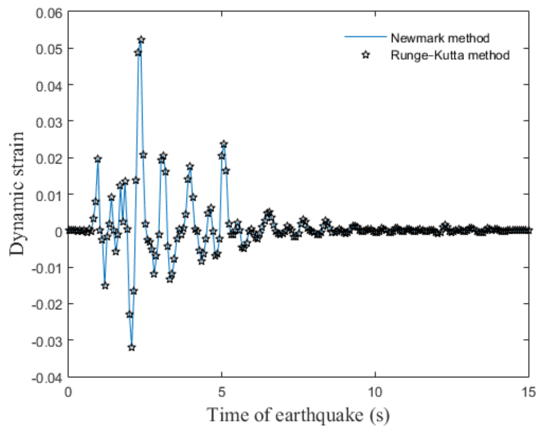

Fig. 3(b) Effect of nanoparticle volume fraction upon dynamic strain

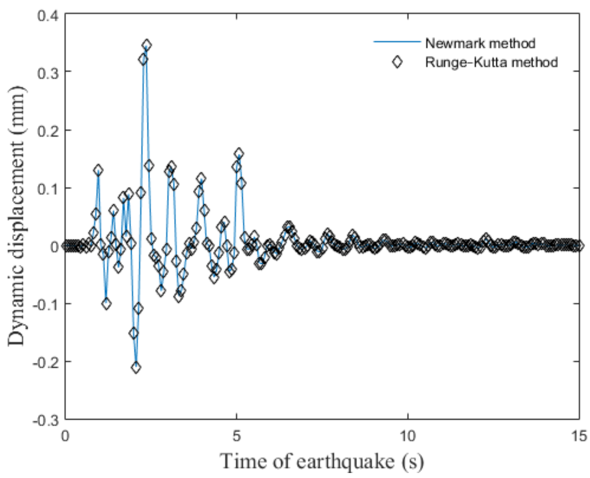

Fig. 3(c) Effect of nanoparticle volume fraction upon dynamic displacement

4.1 Validation

So as to validate the results without neglecting

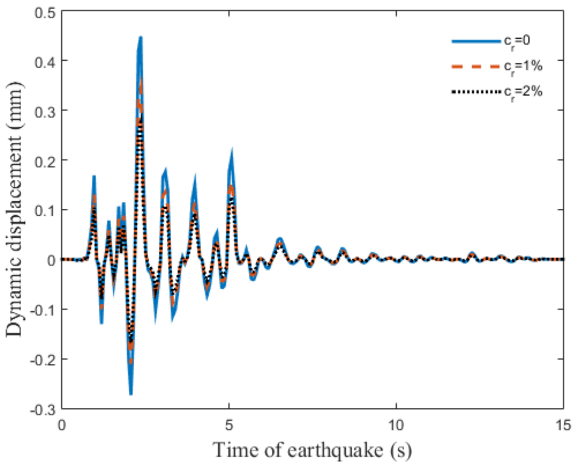

Fig. 4(a) Effect of nanoparticle volume fraction upon dynamic displacement

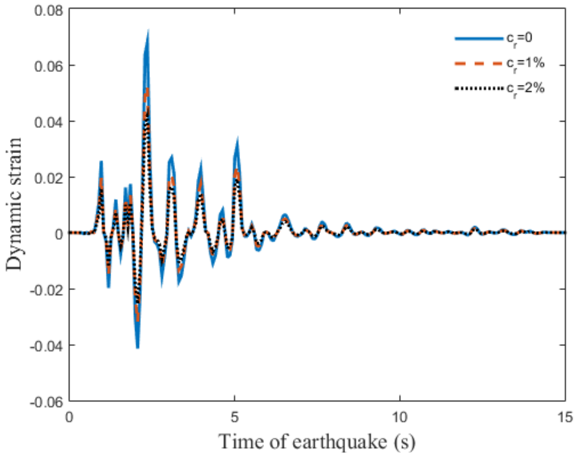

Fig. 4(b) Effect of nanoparticle volume fraction upon dynamic strain

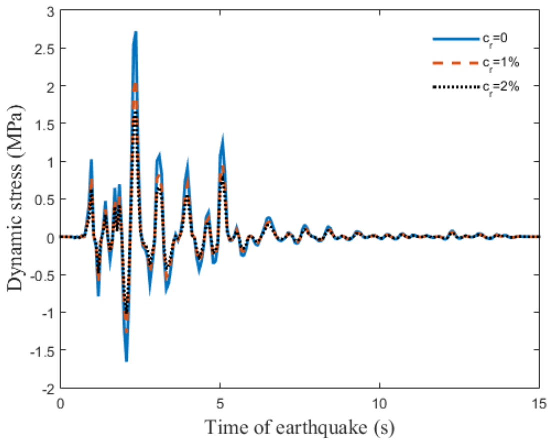

Fig. 4(c) Effect of nanoparticle volume fraction upon dynamic stress

parameters, the Runge-Kutta procedure will be utilized and the gained results are compared with Newmark procedure performed in this paper. Hence, this comparison of results for dynamic stress, strain and displacement respectively are displayed in Figs. 3(a)-3(c). It is transparent that the results for two procedures are in good agreement with each other

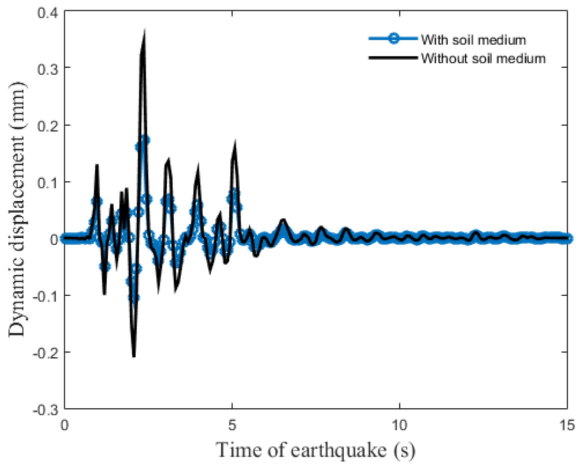

Fig. 5(a) Effect of soil foundation upon dynamic displacement

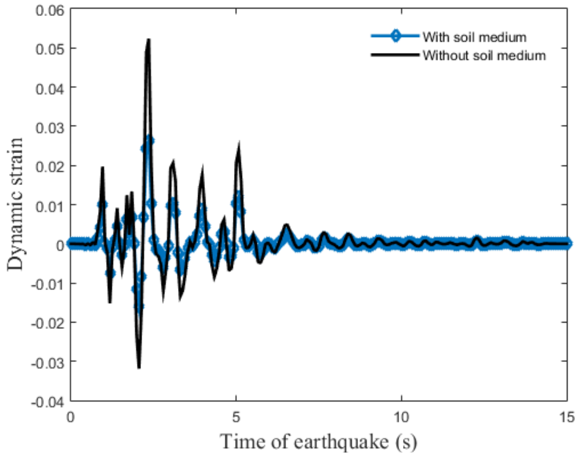

Fig. 5(b) Effect of soil foundation upon dynamic strain

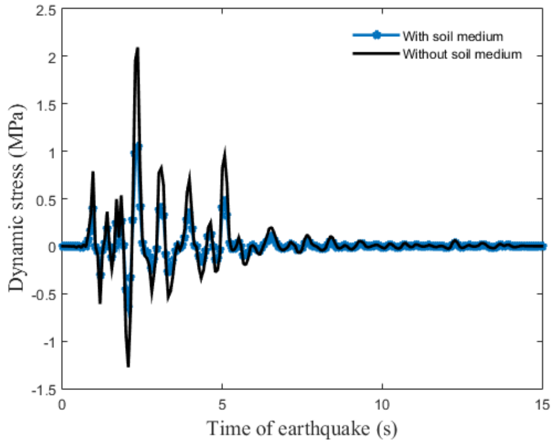

Fig. 5(c) Effect of soil foundation upon dynamic stress

that shows the precision considered numerical method in this research.

4.2 Parametric study

The effect of nanoparticle volume fraction upon dynamic displacement, strain and stress, Figs. 4(a)-4(c) respectively are illustrated. As observed, rise of volume

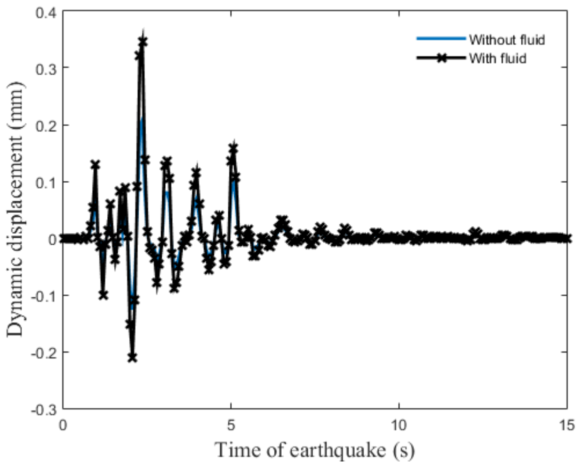

Fig. 6(a) Effect of fluid upon dynamic displacement

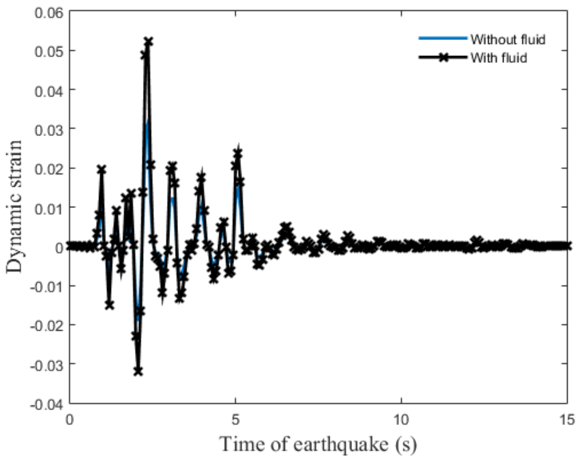

Fig. 6(b) Effect of fluid upon dynamic strain

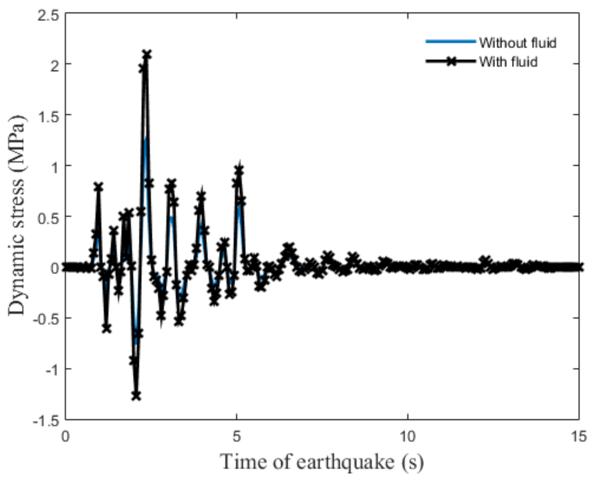

Fig. 6(c) Effect of fluid upon dynamic stress

fraction of nanoparticle leads to diminish the dynamic stress, strain and displacement. It is due to the fact that growth of nanoparticle volume percent causes reduction of pipe instability. Thoroughly, it is determined that with increase in nanoparticle volume fraction about 1%, the dynamic stress, strain and deflection is reduced about 50%.

In order to indicate the effect of soil foundation upon dynamic displacement, strain and stress, Figs. 5(a)-5(c) are

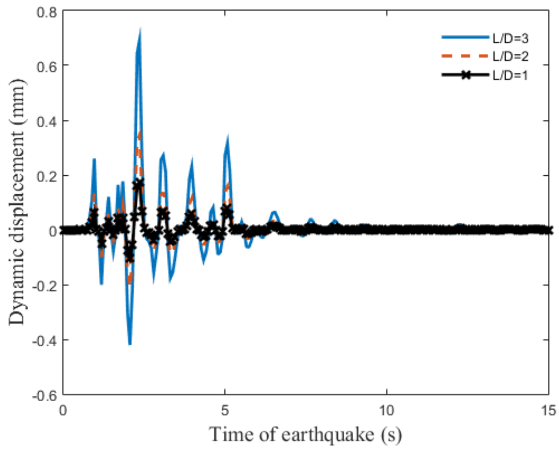

Fig. 7(a) Effect of pipe's length to diameter proportion upon dynamic displacement

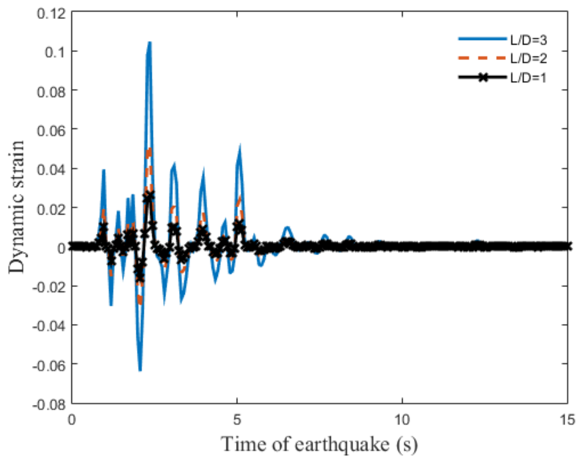

Fig. 7(b) Effect of pipe's length to diameter proportion upon dynamic strain

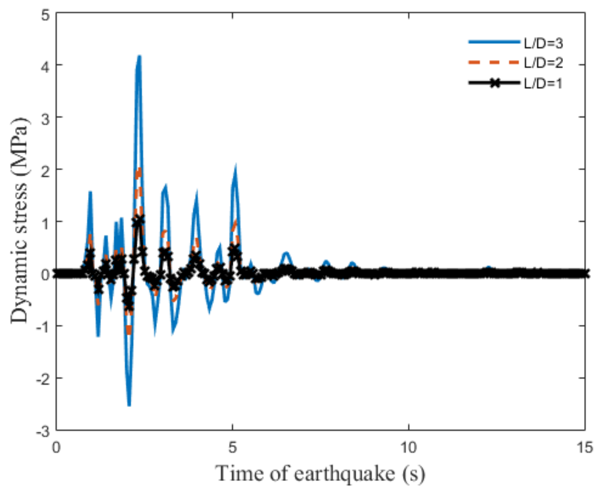

Fig. 7(c) Effect of pipe's length to diameter proportion upon dynamic stress

respectively shown. In this evaluation, two different types of the soil foundation (type of loose sand) are regarded including soil foundation which lacks damping (k_s=4800 N/m^3, c_d=0) and another one which contains damping (k_s=4800 N/m^3, c_d=1000 Ns/m^2). With respect to the figures, considering the soil foundation results in decline of dynamic stress, strain and displacement because of increment of the structure's stiffness. Further, presence of damping adds up to decrease in dynamic stress, strain and displacement, because inducement related to active damp in concrete structure.

Figs. 6(a)-6(c) respectively show the effect of flow of fluid upon the dynamic displacement, strain and stress for concrete structure. It is obvious that passing internal fluid inside the concrete pipe results in increment of dynamic displacement, strain and stress. It can be justified by this reason that conveying internal fluid flow in the concrete pipe generates internal force.

The influence of concrete pipe's length to diameter proportion upon the dynamic displacement, strain and stress are respectively illustrated. As can be seen, increase in length to diameter proportion of this structure causes increment of dynamic stress, strain and deflection. In fact, rise of length to diameter proportion unfavorably affects structure's stiffness.

5. Conclusions

The objective of present research was evaluation of dynamic stress, strain and displacement related to concrete pipe carrying water-based fluid. Moreover, this concrete pipe has been buried in soil and modeled via damper as well as spring elements. Well-known equation of Navier-Stokes was used to count the induced force through fluid. In order to model this concrete structure mathematically, the refined higher order shear deformation theory of shell was applied and using energy method, governing equations were derived. With respect to the Newmark and Galerkin procedures, the governing equations were solved and dynamic stress, strain and displacement related to concrete structure were calculated. Distinct variables containing volume percent of nanoparticle, flow of fluid, length to diameter proportion of the pipe, soil medium and damping and their effects upon dynamic stress, strain and deflection were analyzed. it was determined that increase in nanoparticle volume fraction up to 3% leads to decline of the dynamic stress, strain and deflection about 50%. Further, assumption of soil foundation reduces the dynamic stress, strain and displacement. Likewise, passing the internal fluid inside concrete pipe results in increase in the dynamic stress, strain and displacement.

References

Al Rikabi, F., Sargand, S. and Kurdziel, J. (2019), "Evaluation of synthetic fiber reinforced concrete pipe performance using three-edge bearing test", *J. Test. Eval.*, **47**, 942-958. https://doi.org/10.1520/JTE20170369.

Azmi, M., kolahchi, R. and Rabani Bidgoli, M. (2019), "Dynamic analysis of concrete column reinforced with Sio_2 nanoparticles subjected to blast load", *Adv. Concrete Constr.*, **7**, 51-63. https://doi.org/10.12989/acc.2019.7.1.051.

Belardi, V.G., Fanelli, P. and Vivio. F. (2018). "Bending analysis with Galerkin method of rectilinear orthotropic composite circular plates subject to transversal load", *Compos. B. Eng.*, **140**, 250-259. https://doi.org/10.1016/j.compositesb.2017.12.011.

Bowles, J.E. (1988), *Foundation Analysis and Design*, USA.

Feng, Q., Kong, Q., Huo, L. and Song, G. (2015), "Crack detection and leakage monitoring on reinforced concrete pipe", *Smart. Mater. Struct.*, **24**, 115020.

Goldaran, R., Turer, A., Kouhdaragh, M. and Ozlutas, K. (2020), "Identification of corrosion in a prestressed concrete pipe utilizing acoustic emission technique", *Constr. Build. Mater.*, **242**, 118053. https://doi.org/10.1016/j.conbuildmat.2020.118053.

Hajmohammad, M.H., Maleki, M. and Kolahchi, R. (2018), "Seismic response of underwater concrete pipes conveying fluid covered with nano-fiber reinforced polymer layer", *Soil. Dyn. Earthq. Eng.*, **110**, 18-27. https://doi.org/10.1016/j.soildyn.2018.04.002.

Heydari Nosrat Abadi, M. and Zamani Nouri, A. (2019), "Numerical study for critical fluid velocity in temperature-dependent pipes conveying fluid mixed with nanoparticles using higher order shear deformation theory", *Ship. Offshore. Struct.*, **14**, 501-509. https://doi.org/10.1080/17445302.2018.1512357.

Hua, H., Liao, Z. and Zhang, X. (2018), "The self-excited vibrations of an axially retracting cantilever beam using the Galerkin method with fitted polynomial basis functions", *J. Mech. Sci. Technol.*, **32**, 29-36. https://doi.org/10.1007/s12206-017-1204-z.

Karimi, M. and Shahidi, A. (2018), "Buckling analysis of skew magneto-electro-thermo-elastic nanoplates considering surface energy layers and utilizing the Galerkin method", *Appl. Phys. A-Mater.*, **124**(10), 681. https://doi.org/10.1007/s00339-018-2088-1.

Katariya, P.V., Panda, S.K., Hirwani, C.K., Mehar, K. and Thakare, O. (2017), "Enhancement of thermal buckling strength of laminated sandwich composite panel structure embedded with shape memory alloy fibre", *Smart. Struct. Syst.*, **20**, 595-605. https://doi.org/10.12989/sss.2017.20.5.595.

Kormanikova, E. and Kotrasova, K. (2018), "Multiscale modeling of liquid storage laminated composite cylindrical tank under seismic load", *Compos. B. Eng.*, **146**, 189-197. https://doi.org/10.1016/j.compositesb.2018.03.011.

Looi, D.T.W., Su, R.K.L., Cheng, B. and Tsang, H.H. (2017), "Effects of axial load on seismic performance of reinforced concrete walls with short shear span", *Eng. Struct.*, **151**, 312-325. https://doi.org/10.1016/j.engstruct.2017.08.030.

Luo, L., Nguyen, H., Alabduljabbar, H., Alaskar, A., Alrshoudi, F., Alyousef, R., ... & Dang, H.M. (2020), "Depiction of concrete structures with seismic separation under faraway fault earthquakes", *Adv. Concrete Constr.*, **9**, 71-82. https://doi.org/10.12989/.2020.9.1.071.

Ma, H. and Zhang, D. (2016), "Seismic response of a prestressed concrete wind turbine tower", *Int. J. Civil Eng.*, **14**, 561-571. https://doi.org/10.1007/s40999-016-0029-y.

Mehar, K. and Panda, S.K. (2017), "Thermal free vibration behavior of FG-CNT reinforced sandwich curved panel using finite element method", *Polym. Compos.*, **39**, 2751-2764. https://doi.org/10.1002/pc.24266.

Mehar, K., Panda, S.K. and Mahapatra, T.R. (2017), "Thermoelastic nonlinear frequency analysis of CNT reinforced functionally graded sandwich structure", *Eur. J. Mech. A/Solid.*, **65**, 384-396. https://doi.org/10.1016/j.euromechsol.2017.05.005.

Mehar, K., Panda, S.K., Bui, T.Q. and Mahapatra, T.R. (2017), "Nonlinear thermoelastic frequency analysis of functionally graded CNT-reinforced single/doubly curved shallow shell panels by FEM", *J. Them. Stress.*, **40**, 899-916. https://doi.org/10.1080/01495739.2017.1318689.

Mehar, K., Panda, S.K., Devarajan, Y. and Choubey, G. (2019), "Numerical buckling analysis of graded CNT-reinforced composite sandwich shell structure under thermal loading", *Compos. Struct.*, **216**, 406-414.

https://doi.org/10.1016/j.compstruct.2019.03.002.
Montuori, R. and Muscati, R. (2017), "Smart and simple design of seismic resistant reinforced concrete frame", *Compos. B. Eng.*, **115**, 360-368. https://doi.org/10.1016/j.compositesb.2016.09.050.
Panda, S.K. and Singh, B.N. (2009), "Thermal post-buckling behaviour of laminated composite cylindrical/hyperboloid shallow shell panel using nonlinear finite element method", *Compos. Struct.*, **91**, 366-374. https://doi.org/10.1016/j.compstruct.2009.06.004.
Panda, S.K. and Singh, B.N. (2013), "Nonlinear finite element analysis of thermal post-buckling vibration of laminated composite shell panel embedded with SMA fibre", *Aerosp. Sci. Technol.*, **29**, 47-57. https://doi.org/10.1016/j.ast.2013.01.007.
Peyvandi, A., Soroushian, P. and Jahangirnejad, S. (2013), "Enhancement of the structural efficiency and performance of concrete pipes through fiber reinforcement", *Constr. Build. Mater.*, **45**, 36-44. https://doi.org/10.1016/j.conbuildmat.2013.03.084.
Rose, J., Grasley, Z., Tang, M., Edwards, M. and Wang, F. (2018), "Accelerated autogenous healing of concrete pipe sections with crack and decalcification damage", *J. Mater. Civil Eng.*, **30**, 04018308. https://doi.org/10.1061/(asce)mt.1943-5533.0002503.
Simsek, M. (2010), "Non-linear vibration analysis of a functionally graded Timoshenko beam under action of a moving harmonic load", *Compos. Struct.*, **92**, 2532-2546. https://doi.org/10.1016/j.compstruct.2010.02.008.
Taherifar, R., Nasr Esfahani, S., Nasr Esfahani, M.H., Chinaei, F. and Mahmoudi, M. (2018), "Seismic response of concrete beam with smart layer using DQ and Newmark methods", *Comput. Concrete*, **21**, 717-726. https://doi.org/10.12989/cac.2018.21.6.717.
Thai, H.T. and Choi, D.H. (2011), "A refined plate theory for functionally graded plates resting on elastic foundation", *Compos. Sci. Technol.*, **71**, 1850-1858. https://doi.org/10.1016/j.compscitech.2011.08.016.
Zamani Nouri, A. (2017), "Mathematical modeling of concrete pipes reinforced with CNTs conveying fluid for vibration and stability analyses", *Comput. Concrete*, **19**, 325-331. https://doi.org/10.12989/cac.2017.19.3.325.
Zamani Nouri, A. (2018), "Seismic response of soil foundation surrounded Fe_2O_3 nanoparticlesreinforced concrete pipes conveying fluid", *Soil Dyn. Earthq. Eng.*, **106**, 53-59. https://doi.org/10.1016/j.soildyn.2017.12.009.

CC

Appendix

By introducing Eq. (9) into Eqs. (12) and (13), the stress resultants yield

$$\begin{bmatrix} N_{xx} \\ N_{\theta\theta} \\ N_{x\theta} \\ M^b_{xx} \\ M^b_{\theta\theta} \\ M^b_{x\theta} \\ M^s_{xx} \\ M^s_{\theta\theta} \\ M^s_{x\theta} \end{bmatrix} = \begin{bmatrix} A_{11} & A_{12} & 0 & B_{11} & B_{12} & 0 & B^s_{11} & B^s_{12} & 0 \\ A_{12} & A_{22} & 0 & B_{12} & B_{22} & 0 & B^s_{12} & B^s_{22} & 0 \\ 0 & 0 & A_{66} & 0 & 0 & B_{66} & 0 & 0 & B^s_{66} \\ B_{11} & B_{12} & 0 & D_{11} & D_{12} & 0 & D^s_{11} & D^s_{12} & 0 \\ B_{12} & B_{22} & 0 & D_{12} & D_{22} & 0 & D^s_{12} & D^s_{22} & 0 \\ 0 & 0 & B_{66} & 0 & 0 & D_{66} & 0 & 0 & D^s_{66} \\ B^s_{11} & B^s_{12} & 0 & D^s_{11} & D^s_{12} & 0 & H^s_{11} & H^s_{12} & 0 \\ B^s_{12} & B^s_{22} & 0 & D^s_{12} & D^s_{22} & 0 & H^s_{12} & H^s_{22} & 0 \\ 0 & 0 & B^s_{66} & 0 & 0 & D^s_{66} & 0 & 0 & H^s_{66} \end{bmatrix} \begin{bmatrix} \partial u / \partial x \\ \partial v / \mathrm{R}\partial\theta \\ \partial u / \mathrm{R}\partial\theta + \partial v / \partial x \\ -\partial^2 w_b / \partial x^2 \\ -\partial^2 w_b / \mathrm{R}^2\partial\theta^2 \\ -2\partial^2 w_b / \mathrm{R}\partial\theta\partial x \\ -\partial^2 w_s / \partial x^2 \\ -\partial^2 w_s / \mathrm{R}^2\partial\theta^2 \\ -2\partial^2 w_s / \mathrm{R}\partial\theta\partial x \end{bmatrix}, \tag{A1}$$

$$\begin{bmatrix} Q_{\theta z} \\ Q_{xz} \end{bmatrix} = \begin{bmatrix} A^s_{44} & 0 \\ 0 & A^s_{55} \end{bmatrix} \begin{bmatrix} -\partial w_s / \mathrm{R}\partial\theta \\ -\partial w_s / \partial x \end{bmatrix}, \tag{A2}$$

where

$$\left(A_{ij}, B_{ij}, D_{ij}, E_{ij}, F_{ij}, H_{ij}\right) = \int_{-h/2}^{h/2} \left(1, z, z^2, z^3, z^4, z^5, z^6\right) C_{ij} dz, \quad (i, j = 1,2,4,5,6) \tag{A3}$$

$$B^s_{ij} = -\frac{1}{4}\mathrm{B}_{ij} + \frac{5}{3h^2}E_{ij}, \tag{A4}$$

$$D^s_{ij} = -\frac{1}{4}D_{ij} + \frac{5}{3h^2}F_{ij}, \tag{A5}$$

$$H^s_{ij} = \frac{1}{16}D_{ij} - \frac{5}{6h^2}F_{ij} + \frac{25}{9h^4}H_{ij}, \tag{A6}$$

$$A^s_{ij} = \frac{25}{16}A_{ij} - \frac{25}{2h^2}D_{ij} + \frac{25}{h^4}F_{ij}, \tag{A7}$$